AD-A137 523 CLOSED LOOP ADAPTIVE CONTROL OF A 40 GIGAHERTZ REACTIVELY STEERED MICROST..(U) NAVAL WEAPONS CENTER CHINA LAKE CA R J DINGER OCT 83 NWC-TP-6481 1/1

UNCLASSIFIED SBI-AD-E900 294 F/G 9/5 NL

END

DATE FILMED

3-84

DTIC

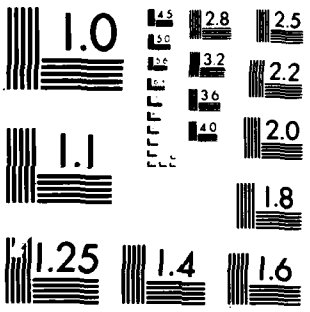

NWC TP 6481

13

Closed Loop Adaptive Control of a 4.0 Gigahertz Reactively Steered Microstrip Array: Experimental Results,

by
R. J. Dinger
Research Department

OCTOBER 1983

NAVAL WEAPONS CENTER
CHINA LAKE, CALIFORNIA 93555

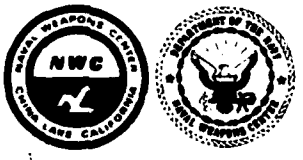

Naval Weapons Center
AN ACTIVITY OF THE NAVAL MATERIAL COMMAND

FOREWORD

The research described in this report was performed during Fiscal Year 1983 and was supported by Independent Research and Independent Exploratory Development funding. It is part of a continuing effort to explore novel radio frequency radiating and receiving structures for applications to airborne communications and radar systems.

W. Woodworth and M. Ronning have reviewed the report for technical accuracy.

Approved by
E. B. ROYCE, Head
Research Department
6 October 1983

Under authority of
K. A. DICKERSON
Capt., U. S. Navy
Commander

Released for publication by
B. W. HAYS
Technical Director

NWC Technical Publication 6481

Published by . . . . . Technical Information Department
Collation . . . . . Cover, 13 leaves
First printing . . . . . 130 copies

UNCLASSIFIED

SECURITY CLASSIFICATION OF THIS PAGE (When Data Entered)

REPORT DOCUMENTATION PAGE	READ INSTRUCTIONS BEFORE COMPLETING FORM
1. REPORT NUMBER: NWC TP 6481	2. GOVT ACCESSION NO. A1 [illegible]
	3. RECIPIENT'S CATALOG NUMBER
4. TITLE (and Subtitle): CLOSED LOOP ADAPTIVE CONTROL OF A 4.0 GIGAHERTZ REACTIVELY STEERED MICROSTRIP ARRAY: EXPERIMENTAL RESULTS,	5. TYPE OF REPORT & PERIOD COVERED: Interim Report on continuing problem
	6. PERFORMING ORG. REPORT NUMBER
7. AUTHOR(s): R. J. Dinger	8. CONTRACT OR GRANT NUMBER(s)
9. PERFORMING ORGANIZATION NAME AND ADDRESS: Naval Weapons Center, China Lake, CA 93555	10. PROGRAM ELEMENT, PROJECT, TASK AREA & WORK UNIT NUMBERS: 61152N; 62766N
11. CONTROLLING OFFICE NAME AND ADDRESS: Naval Weapons Center, China Lake, CA 93555	12. REPORT DATE: October 1983
	13. NUMBER OF PAGES: 22
14. MONITORING AGENCY NAME & ADDRESS (if different from Controlling Office)	15. SECURITY CLASS. (of this report): UNCLASSIFIED
	15a. DECLASSIFICATION DOWNGRADING SCHEDULE

16. DISTRIBUTION STATEMENT (of this Report)

Approved for public release; distribution unlimited.

17. DISTRIBUTION STATEMENT (of the abstract entered in Block 20, if different from Report)

18. SUPPLEMENTARY NOTES

19. KEY WORDS (Continue on reverse side if necessary and identify by block number)

Adaptive Arrays
Anti-jam Techniques
Microstrip Antennas
Optimization Techniques
Parasitic Antennas

20. ABSTRACT (Continue on reverse side if necessary and identify by block number)

See back of form.

DD FORM 1 JAN 73 1473 EDITION OF 1 NOV 65 IS OBSOLETE
S/N 0102-LF-014-6601

UNCLASSIFIED

SECURITY CLASSIFICATION OF THIS PAGE (When Data Entered)

(U) Closed Loop Adaptive Control of a 4.0 Gigahertz Reactively Steered Microstrip Array: Experimental Results, by R. J. Dinger. China Lake, Calif., Naval Weapons Center, October 1983. 22 pp. (NWC TP 6481, publication UNCLASSIFIED.)

(U) A reactively steered adaptive array (RESAA) has one element connected by a transmission line to a receiver and a number of closely spaced parasitic elements, each of which is terminated by an adjustable reactive load. The pattern is formed by control of the reactive loads. Experimental results are presented for a linear RESAA consisting of five microstrip rectangular patch elements resonant at 4.0 GHz. Using steepest descent control of the reactive loads in a power inversion mode (no reference), we find that a null with a depth of 30 dB (relative to the pattern maximum) and an angular width of about 25 degrees can be steered towards an interferer. Typically, about 40 steps (iterations) or less are needed for forming the null. For the power meter and general purpose minicomputer that served as the controller, adaptation times of several seconds are required; extrapolation to a dedicated microprocessor controller predicts adaptation times of several milliseconds. Operation in a mode using a reference signal demonstrates that the pattern can be shaped to steer a null towards interference and a lobe towards a desired signal. A steepest ascent technique (with no reference) was able to form a beam of modest directivity (7 dB) towards a desired signal. The nulling bandwidth is approximately 20 MHz with this array. The advantages of a RESAA, as compared with a conventional adaptive array, include the elimination of the mixers and other hardware needed to perform the complex weighting of the output of each element at an intermediate frequency and smaller overall array size.

CONTENTS

INTRODUCTION

A reactively steered adaptive array (RESAA), shown in Figure 1, has only a single element that is connected by a transmission line to a receiver. The remaining elements are parasitic, and the pattern is formed according to the values of the reactive terminations on these parasitic elements. In an earlier report[1] we described work on a RESAA consisting of five microstrip patch elements resonant at 4.0 GHz. That report developed an equation for the pattern of the array and presented the results of a series of computer simulations of the array performance using a steepest descent[2] algorithm for control. The only experimental results presented in the earlier report were antenna patterns formed by manual adjustment of the reactive loads; these patterns principally served to demonstrate that a significant degree of pattern control is possible in a microstrip patch array by varying the reactive loads on parasitic elements.

This report presents experimental results for this same array as controlled automatically in an adaptive feedback loop. Both the array and the reactive loads (varactor phase shifters) are identical to those shown in Reference 1. Adaptive processing based on a steepest descent algorithm similar to the one investigated in the earlier simulations[1] is used with a minicomputer on an antenna range to demonstrate closed loop control. Both a power inversion mode (nulling of an incident signal without a reference) and a mode that uses a synchronous reference to separate a desired signal from an interferer are investigated. In addition, measurements are described that use a steepest ascent algorithm to form a beam towards a desired signal.

We find that a null with a depth greater than 30 dB (relative to the pattern maximum) and a width of about 25 degrees can be steered toward an interferer. Typically, no more than 40 steps (iterations) are needed to form the null; with the relatively slow general purpose minicomputer that served as the controller (with programming in Fortran), adaptation times of several seconds were achieved. With a synchronous reference, a null can be steered towards an undesired interference source and a pattern maximum can be steered simultaneously towards a desired signal. Steepest ascent beam steering produces a beam with a directivity of about 7 dB.

---

[1] Naval Weapons Center. Reactively Steered Adaptive Array Using Microstrip Patch Elements at 4 Gigahertz, by R. J. Dinger. China Lake, Calif., NWC, February 1983. (NWC TP 6421, publication UNCLASSIFIED.)

[2] G. A. Bekey and W. J. Karplus. Hybrid Computation. New York, John Wiley and Sons, 1969. Pp. 270-280.

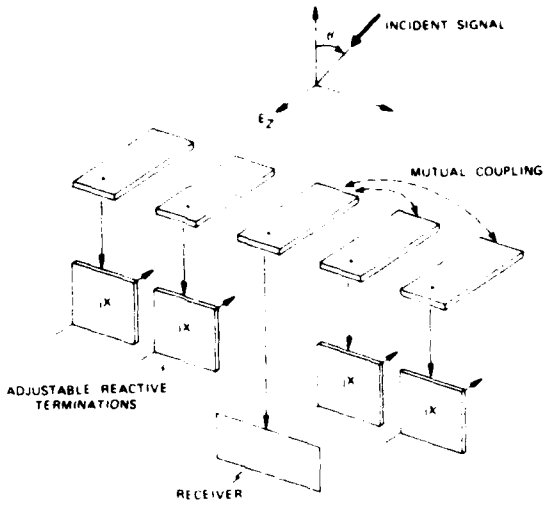

FIGURE 1. Diagram of Reactively Steered Array. The pictured elements represent the microstrip patches of the experimental array (minus the ground plane). The geometry for the pattern measurements is also shown.

ARRAY AND TEST CONFIGURATION

ARRAY DESIGN

The experimental array, shown in Figure 2, consists of five microstrip rectangular patch elements. Each element measured 1.0 x 2.33 cm and was resonant at 4.0 GHz. The edge-to-edge separation was 0.75 cm, corresponding to a separation of 0.1λ at 4.0 GHz. The substrate material was Rexolite 1422 with a thickness of 1.58 mm and a dielectric constant of 2.50.

REACTIVE LOAD DESIGN

A variable reflection phase shifter terminating a transmission line with a characteristic impedance Z produces a variable reactance X given by $X = Z \tan\phi$, where ϕ is the phase shift. Microstrip phase shifters were designed and fabricated to provide the necessary amount of phase shift, using a varactor diode mounted between a 50-ohm microstrip line and the ground plane. Approximately 250 degrees of phase shift could be obtained with a bias voltage range of 0 to -10 V. These phase shifters were the same units used for the manual control measurements presented in Reference 1.

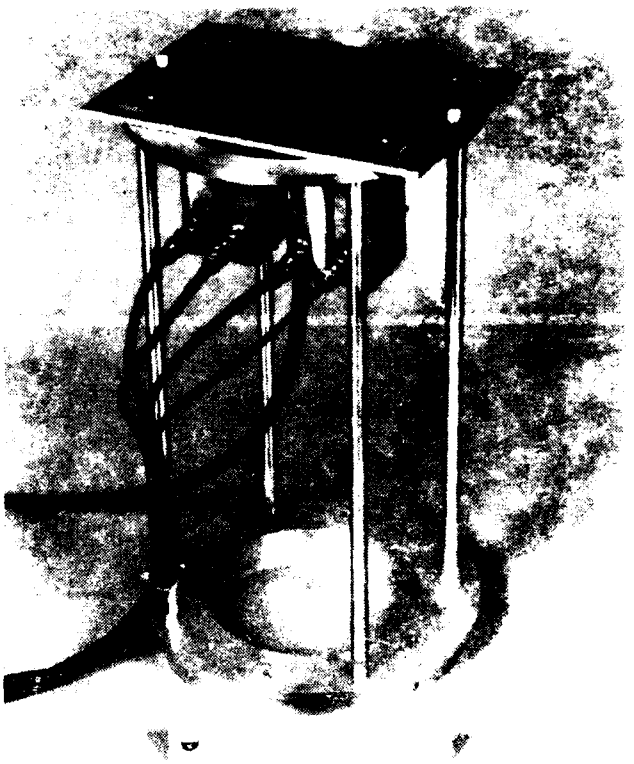

FIGURE 2. Experimental Antenna Array.
Scale in inches.

CLOSED LOOP CONTROLLER AND TEST CONFIGURATION

In Figure 3 we show the array configured for closed loop operation on a roof-top test range. Two distinct operating modes are incorporated in this diagram. With the switches in position A, a power inversion mode (i.e., no reference signal) results; a digital power meter measured the array output and transferred the reading to a Hewlett-Packard HP-1000 computer over an IEEE-488 bus. For most of the measurements in the power inversion mode, only one source radiated, as Figure 3 indicates. With the switches in position B, a reference mode results, in which a narrow band coherent receiver is modeled using a lock-in detector and a reference signal applied both to the lock-in detector and one of the radiating sources (the desired signal). A second radiating source is frequency modulated by a triangle wave, producing a frequency modulation (FM) interference signal whose frequency excursion is centered about the frequency of the desired signal. In this reference mode, the input signal to the computer was obtained from a fast analog-to-digital conversion (20 kHz

conversion rate) of the lock-in detector output voltage. In both modes of operation, the control signals generated by the computer were converted to analog voltages with a range of 0 to -10 V and applied to the varactor bias port of the phase shifters. For the power inversion mode, the speed of the control loop was dominated both by the integration time of the power meter and the slow transfer rate of the IEEE-488 bus; for these reasons, the results are presented in terms of the number of iterations rather than absolute time. The reference mode was substantially faster because a relatively short integration time on the lock-in detector (1 msec) was used and no IEEE-488 bus was required.

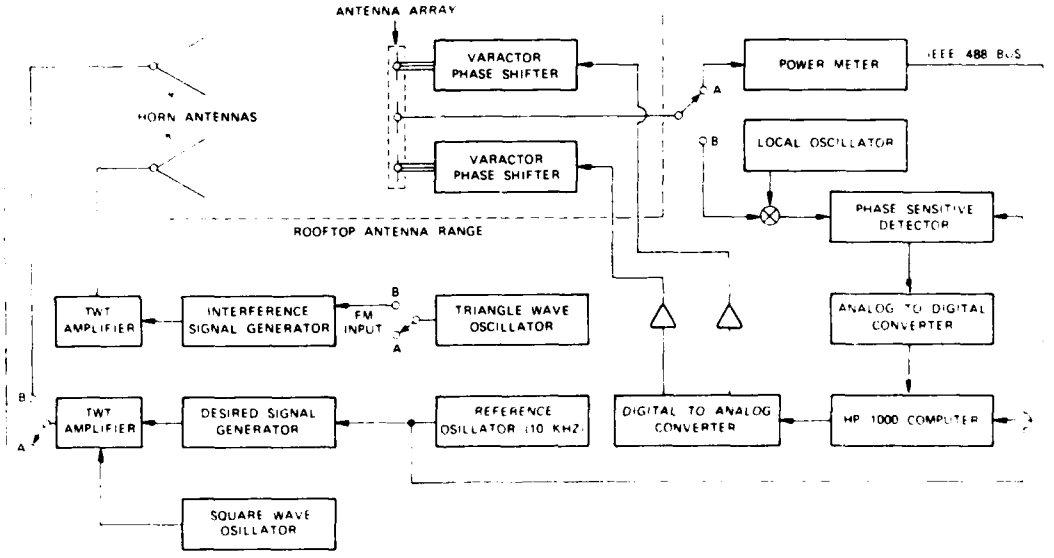

FIGURE 3. Diagram of Test Setup.

POWER INVERSION RESULTS

CONTROL ALGORITHM

The control algorithm, written in Fortran on the HP-1000 computer, was a straightforward implementation of the discrete steepest descent method used in the simulations in Reference 1. Letting $X_i(j)$ denote the reactive load on the ith antenna at the jth iteration, the discrete steepest descent algorithm states that the reactive load at the next iteration, $X_i(j+1)$, is given by

$$X_i(j+1) = X_i(j) - K\nabla\varepsilon \qquad (1)$$

where K is a positive constant that controls the convergence rate, and ε is an N-dimensional error criterion (N = total number of elements). Rather than make a true measurement of all components of the gradient, however, at each iteration only one of the reactive loads was incremented by a small amount (referred to as the step size, below) and the change noted in the array output. If the array output was lowered, the next load was incremented and the array output measured, and so on sequentially and repeatedly through all of the terminations. When an incremental change produced an increase in the array output, the sign of the load increment was changed. In the Appendix a flow chart and detailed description of the algorithm are given.

We made numerous runs to investigate the effects of signal incidence angle, step size, feedback constant K (Equation 1), and termination initial values. In Figures 4 through 15 we show a selection of typical results. For all of these curves, we have used a value of K = 0.10 V^2/mW (the units take this form because the reactive loads are controlled by the bias voltage and not by any measure of the load reactance). We found this value to be a good compromise between excessive steady state fluctuations and a convergence that was too slow.

INTERFERENCE NULLING

For Figure 4 we positioned the array so that the signal was incident at θ = 0 degrees (broadside) and set the initial values of the terminations to a uniform value (-4.0 and -2.0 V). The time history of the decrease in array output is shown; for initial values of -4.0 V, about 40 iterations are needed to decrease the power from the initial -20 dBm to a final value of about -55 dBm. At the nulling point the fluctuation in array output is about 10 dB, a typical result. For initial values of -2.0 V, the nulling is substantially poorer, with only about a 15 dB decrease in the array output realized. In general, we found that an initial point of -4.0 V for all terminations guaranteed a signal reduction of at least 30 dB for incidence angles of 45 to -45 degrees, usually within about 40 iterations. The nulling ability, as measured by the difference between the "before" and "after" array outputs, became smaller as the incidence angle approached grazing incidence (90 and -90 degrees), principally because the quiescent pattern prior to adaptation was naturally smaller in those directions to begin with.

Figure 5 displays the variation of the terminations during the -4.0 V curve of Figure 4. The step size of 0.1 V and the method of sequentially testing for a decrease in array output are evident in these curves. The approach to a steady state value for each termination and a small "wander" in the steady state value can also be seen.

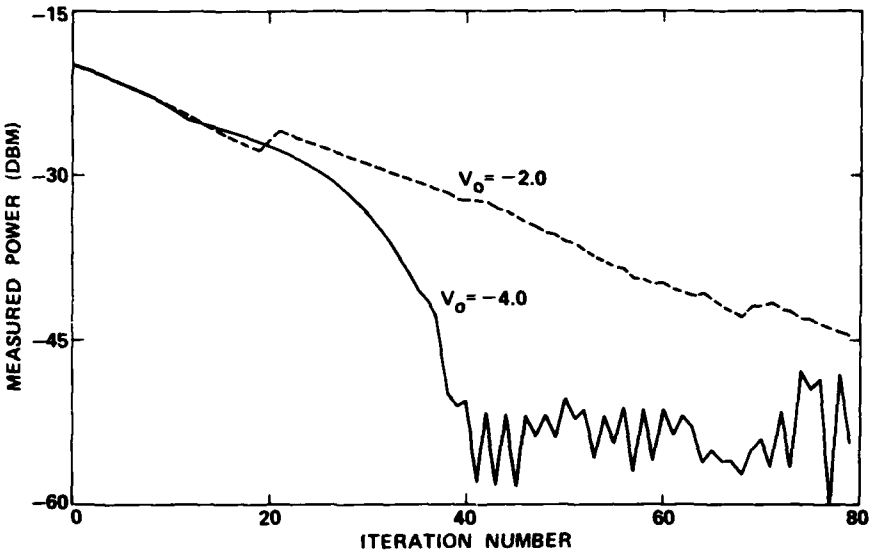

FIGURE 4. Variation of Array Output Power During Nulling of Signal Incident at θ = 0 Degrees. Curves for two initial reactive load values (-2.0 and -4.0 V bias on the varactor diodes) are shown.

Another approach to selecting the initial point is to conduct a random search phase. In this scheme, termination values are selected by a uniform random number generator, and the values producing the lowest array output at the end of the random search phase are entered as the intital values for the steepest descent algorithm. In Figure 6 we show a power reduction curve in which a 10-step random search phase is followed by steepest descent processing. For this example, the total number of steps to decrease the power from -20 dBm to -50 dBm is about one-half the number required when starting with -4.0 V on all terminations (Figure 4), a typical result; we have also found that the use of a random search phase usually produces a deeper null with smaller steady state fluctuations.

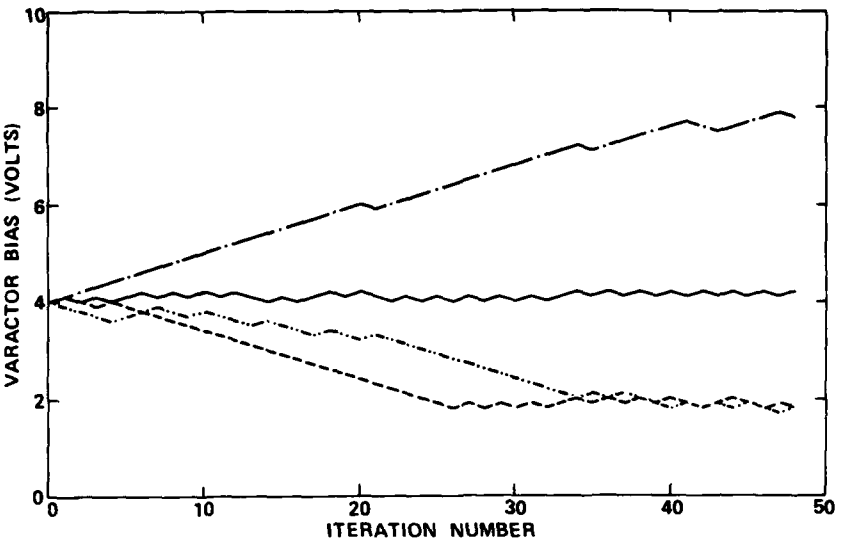

FIGURE 5. Variation of the Four Reactive Terminations During the Signal Nulling Shown in Figure 4 for V_o = -4.0 V.

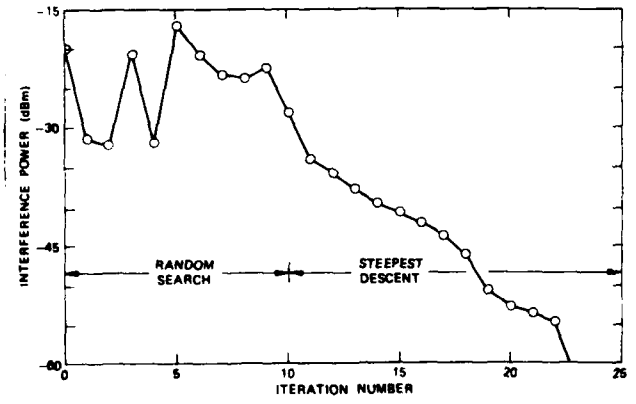

FIGURE 6. Nulling Produced by Random Search Followed by Steepest Descent Processing.

In Figures 7 and 8 we plot typical antenna radiation patterns, showing the formation of a null towards the interference signal. Figure 7 includes three traces to demonstrate that although the termination values necessary to produce a null in a given direction are not unique (i.e., many local minima occur in the error surfaces), the radiation patterns for all the possible solutions are remarkably similar. Three radiation patterns produced by the three sets of termination values that null a broadside signal are shown; the termination values, which are listed in Table 1, were arrived at by starting with different initial values.

TABLE 1. Values of the Reactive Load Bias Voltage (in Volts) for the Three Curves Shown in Figure 7. Element 3 is the center element connected to the receiver.

	Curve A (solid)	Curve B (dashed)	Curve C (dot-dashed)
Element 1	-0.16	-9.28	-3.68
Element 2	-5.96	-8.51	-6.55
Element 4	-3.53	-4.05	-0.69
Element 5	-5.56	-7.13	-5.83

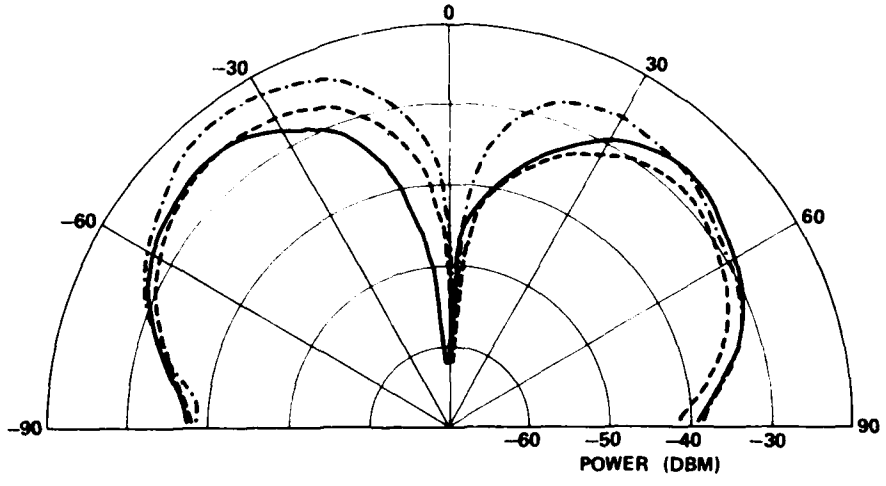

FIGURE 7. E-Plane Antenna Patterns for Interference Incident at θ = 0 Degrees Resulting after Nulling. The three patterns shown are produced by the three sets of reactive termination values listed in Table 1. A power level of -20 dBm corresponds to 7 dBi.

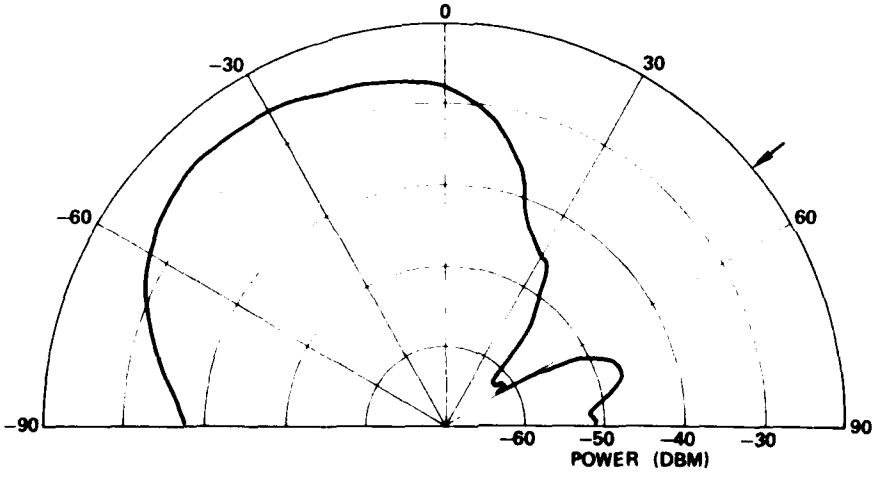

FIGURE 8. E-Plane Antenna Pattern for Interference Incident from Angle Indicated by Arrow after Nulling.

INTERFERENCE NULLING WITH A THREE-ELEMENT ARRAY

As the number of parasitic elements increases, the depth of the null should increase and the width should narrow up to a point. Figure 9 shows a null formed at broadside in which the loads on the outer elements (i.e., elements 1 and 5) were removed and only the loads on the inner parasitic elements (2 and 4) were adjusted. The null formed by the three-element array has a depth of only 18 dB below the pattern maximum and the width is about 60 degrees at 10 dB below the pattern maximum, compared to 30 dB and 25 degrees, respectively, (Figure 8) for a five-element array. The addition of two more parasitic elements clearly gives a substantial improvement in performance. As the number of elements is increased beyond five, however, at some point the influence of the additional elements added at the periphery will begin to have a negligible effect on the pattern. The number of elements for "diminishing returns" will be found experimentally in future work on this program.

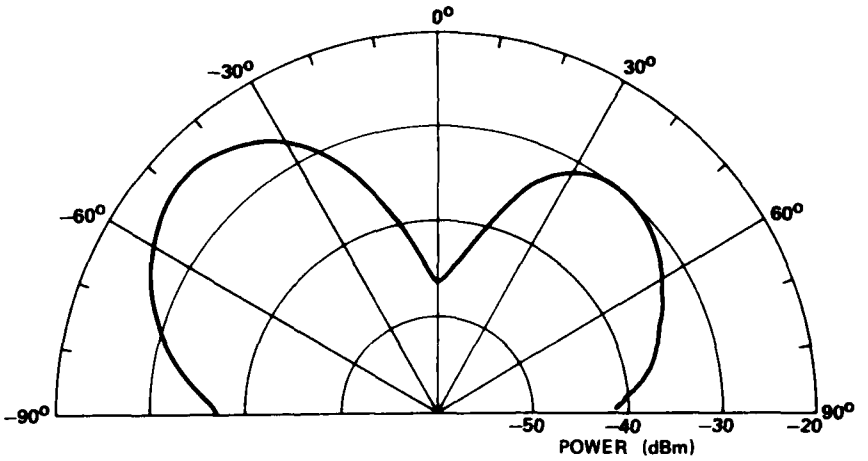

FIGURE 9. E-Plane Antenna Pattern for Three-Element Array for Interference Angle Incident at 0 Degrees.

PROBABILITY DENSITY FUNCTION OF THE CONTROL SURFACE

The "control surface" for a RESAA, a useful concept for visualizing its convergence properties, is the N-dimensional surface produced by the receiver output as the terminations on the (N-1) parasitic elements are varied over their range of control. For a three-element array, the control surface can be easily displayed in a three-dimensional perspective drawing (in Reference 1 theoretical

surfaces were presented for a three-element array); however, for more than three elements, the surface cannot be so easily visualized.

One way to picture the surface is to plot the probability density function (PDF) of the receiver output for randomly selected loads. In Figure 10 we plot the PDFs for the five-element RESAA for signals incident at 0 and 45 degrees, as determined from 1000 samples. These curves show that the most probable output power of the array for randomly selected loads is about -24 dBm, but that there exists a set of loads that can produce a power of as large as -17 dBm (corresponding to lobe steering towards the incident signal) or as small as -54 dBm (null steering). The goal of a nulling algorithm, of course, is to arrive in an expeditious manner at the loads that produce the -54 dB tail in the PDF. Figure 10 does not indicate how many fundamentally different sets of loads produced the tail, i.e., does not show how many local minima exist in the control surface.

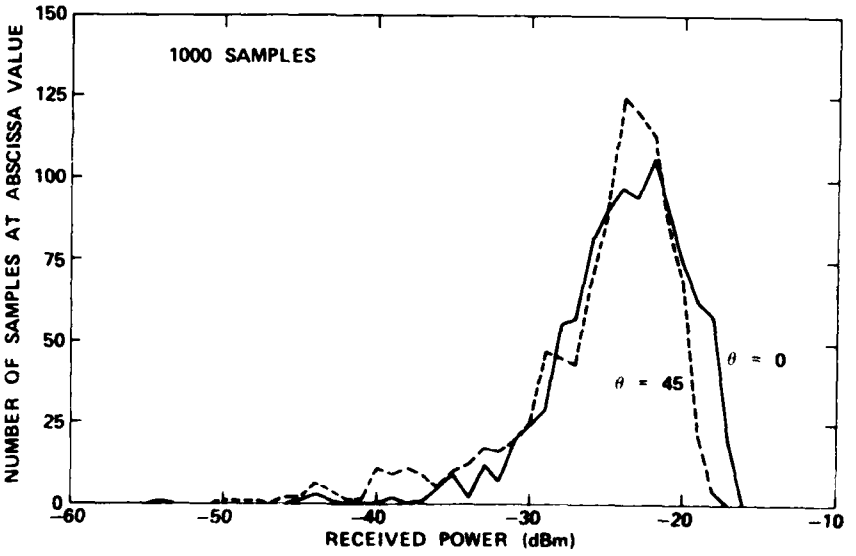

FIGURE 10. Probability Density Function (Fraction of Samples--1000 Total--at Each Abscissa Value for Uniformity Distributed Random Load Values) for Two Angles of Incidence.

Figure 11 plots the cumulative distribution function (CDF) for the PDFs in Figure 10. As an example of how to interpret these curves, Figure 11 implies that for broadside incidence a purely random search control algorithm has a probability of (5/1000) = 0.005 of decreasing a signal to at least -40 dBm with a single sample.

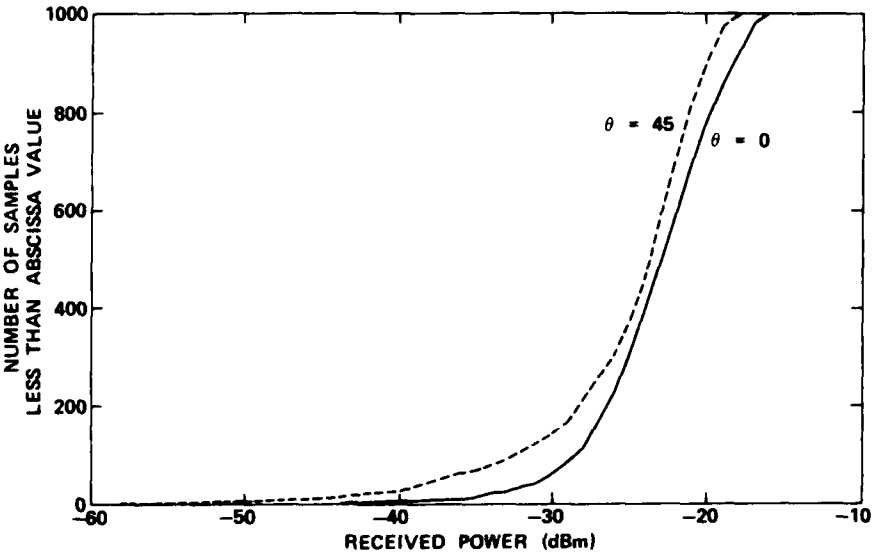

FIGURE 11. Cumulative Distribution Function for Data Given in Figure 10.

NULLING BANDWIDTH

In Figure 12 we give an example of the frequency response of the array. The signal was nulled at a frequency of 4.0 GHz, the termination values were held constant, and the source frequency was then swept. Defining the nulling bandwidth as the frequency interval over which the null is at least 20 dB below the pattern maximum, a value of about 20 MHz is obtained for this array. The nulling bandwidth is determined by the array configuration (primarily the spacing between the elements) and the bandwidth of the reactive loads. The varactor phase shifters were not designed to optimize bandwidth; with a more elaborate design (perhaps by using a circulator and multiple PIN diodes to produce a nondispersive phase shifter) the bandwidth of the reactive loads, and hence the nulling bandwidth, can be substantially increased.

The array bandwidth, which we define as the frequency range over which the voltage standing wave ratio (VSWR) at the center element is less than 2.0, is about 100 MHz. This value is typical for microstrip patch elements. Other definitions of array bandwidth could be considered, such as the frequency range over which a null can be formed of a certain depth towards an interferer; however, we have not yet characterized the array in this manner.

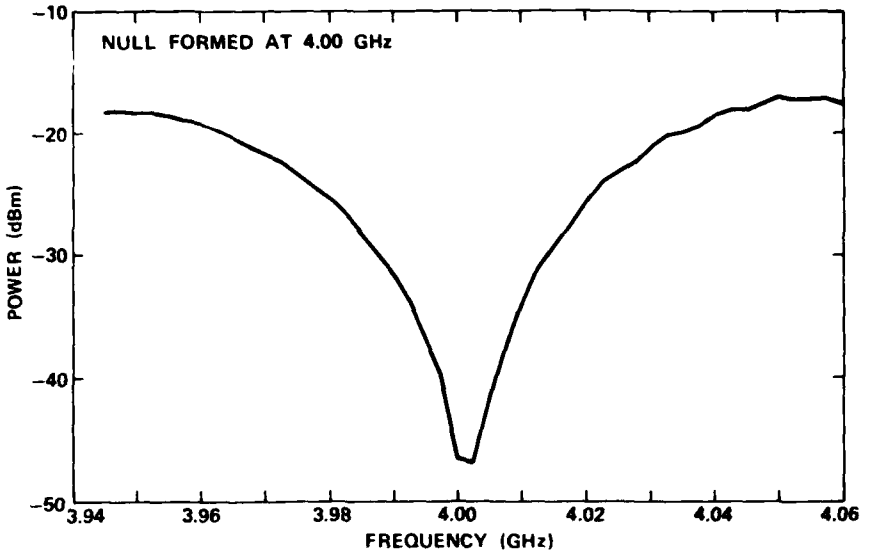

FIGURE 12. Frequency Response of Null for Interference Incident at θ = 0 Degrees.

NULLING DURING ANTENNA ROTATION

The effects of antenna rotation and source movement are displayed in Figure 13. Following the initial nulling of the signal, during which time the antenna was stationary, the antenna was rotated at a rate of one degree for each three iteration steps. The null was tracked over a range of about 40 degrees, at which point a noticeable increase in array output occurs. Comparison with Figure 14, which plots the variation in termination value during the rotation of the antenna, shows that the array output increases because one of the terminations hits the limit at 0.0 V. Sometimes such a limit can be compensated for by changes in the other terminations, but in this particular case compensation did not or could not occur. We have found that a random search phase leads to an initial null that can be tracked over a larger angular change than a null achieved after a start from a uniform set of values (usually -4.0 V).

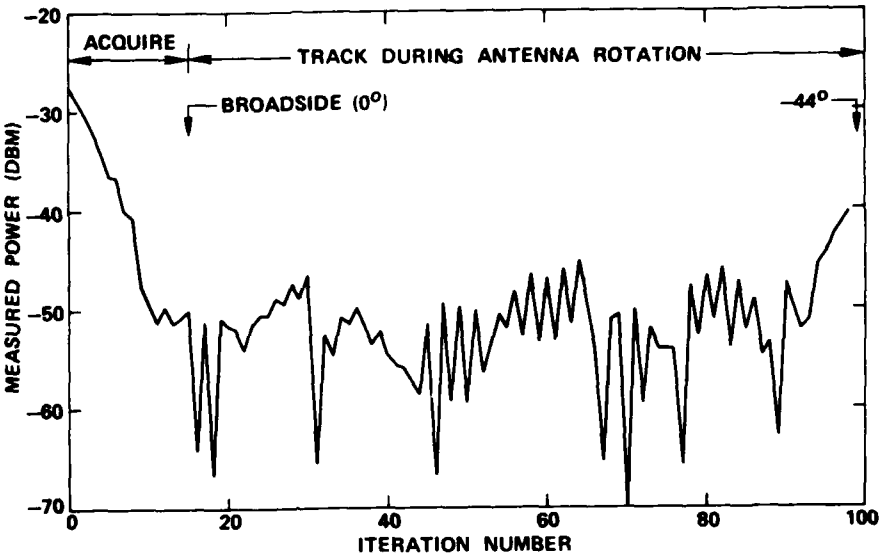

FIGURE 13. Power Received During Nulling Followed by Antenna Rotation.

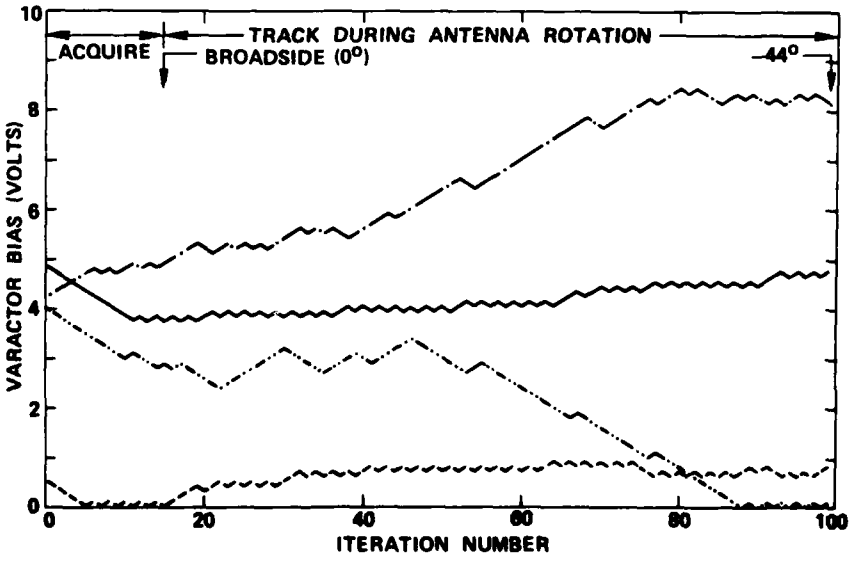

FIGURE 14. Variation of Reactive Terminations During Sequence Given in Figure 13.

Figure 15 is a plot of antenna pattern "snapshots" at various points during the rotation of the antenna. These patterns were obtained by reading off the values of the terminations at the indicated incidence angles during the rotation, fixing these values on the terminations, and then measuring the pattern. The pattern null rotates towards the interference source with relatively little distortion of the pattern at other azimuths.

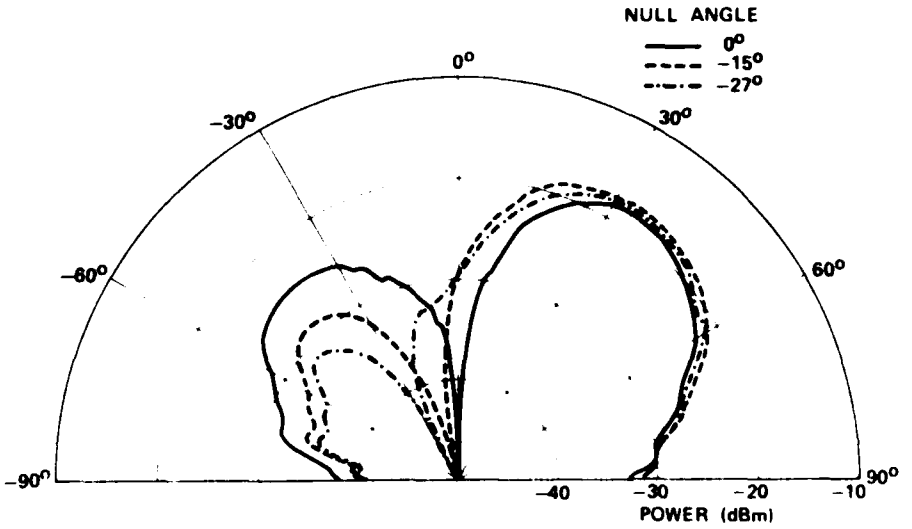

FIGURE 15. E-Plane Antenna Patterns at Selected Points During Rotations of Antenna for Data Presented in Figures 13 and 14.

REFERENCE MODE RESULTS

An FM interference source, whose modulation bandwidth was centered about the 4.0 GHz center frequency of the array, radiated a power that was 20 dB higher than the desired signal (see Figure 3). This interference was sufficient to prevent the lock-in detector from acquiring the desired signal. Figure 16 shows a time history of the array output before adaptation, showing large impulses that occur when the FM source sweeps through the lock-in detector frequency.

The adaptive algorithm used the same steepest descent technique described for the power inversion mode, except that the ratio of the second moment to the average value of the lock-in detector output was minimized. Minimization of this ratio placed a spatial null towards any signal producing an impulsive output and maintained a large pattern value towards any signal that was, by comparison, relatively smooth in its time variation. The post-adaptation trace in Figure 16

and the pattern in Figure 17 show the effect of the adaptive processing. A null was steered towards the FM interference source, and a pattern maximum was maintained towards the desired signal. As indicated in Figure 16, the square wave modulation on the desired signal was recovered.

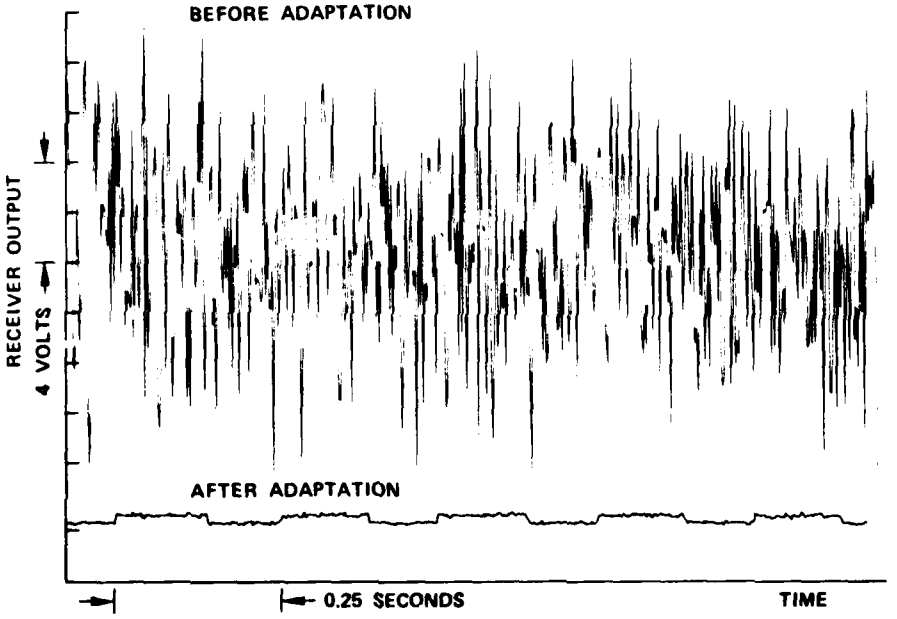

FIGURE 16. Time Traces of Array Output.

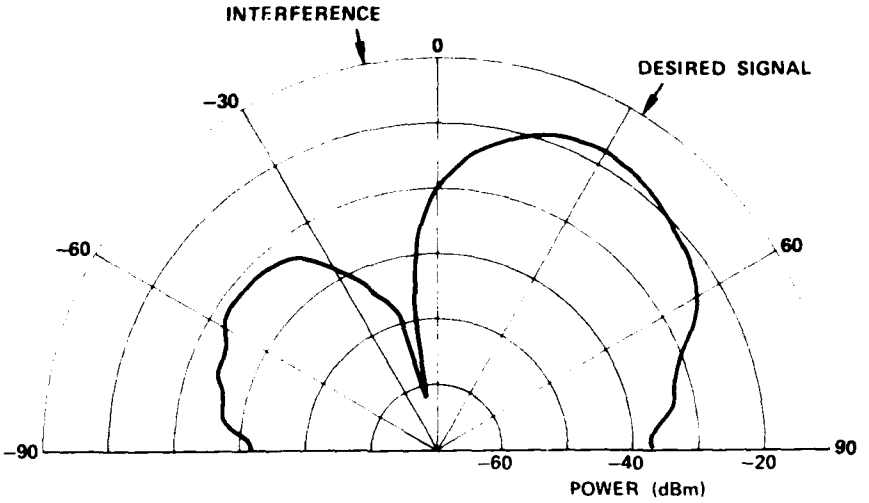

FIGURE 17. E-Plane Antenna Pattern Following Interference Nulling and Lobe Steering Towards a Desired Signal for Time Traces Given in Figure 16.

BEAM STEERING

As shown by Figure 10, the most likely output power of the array for a random selection of termination values is about -24 dBm, but termination values can be found that yield an output of -17 dBm, about 7 dB higher. This result, coupled with the observation that a distinct lobe was formed towards the desired signal in the reference mode measurements of the previous section, suggests that main beam steering can be accomplished with a RESAA.

The patterns in Figures 18(a) and (b) were formed by using a steepest ascent control algorithm to maximize the receiver output. The algorithm (and computer code) is identical to the steepest descent algorithm outlined in the Appendix, except that at each iteration an increase in received power is tested for. Figure 18 shows that pattern maxima with an amplitude of about -17 dBm are formed towards the incident signals, but the directivity (about 7 dB) is relatively low. This directivity is approximately what would be expected for this array (five patch elements of approximately 0.8 λ overall length).

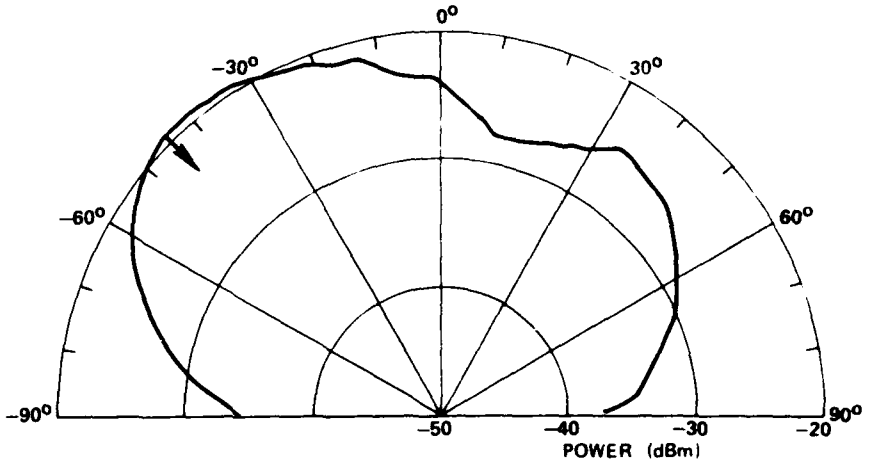

(a)

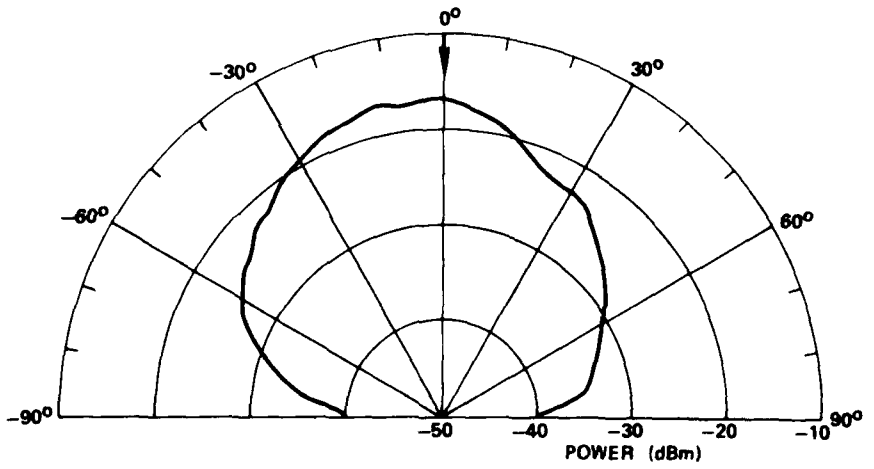

(b)

FIGURE 18. E-Plane Antenna Patterns Formed by a Steepest Ascent Algorithm to Form Pattern Maximum Towards (a) Desired Signal Incident from -45 Degrees and (b) Desired Signal Incident from 0 Degrees.

DISCUSSION AND CONCLUSIONS

The results reported here demonstrate that a useful degree of pattern control of a microstrip adaptive array can be achieved by adjustment of the reactive loads on parasitic elements. Nulls with a

depth greater than 30 dB and a width of about 25 degrees were steered towards an interference source over a bandwidth of about 20 MHz. The same steepest descent algorithm was also able to maintain a null on the interference source during rotation of the array through angles of at least 40 degrees. The pattern was also controlled using a reference to generate a lobe towards a desired signal and a null towards an interference source; a reference signal can be provided by any of the many methods described in the literature. Comparison of results using only two parasitic elements versus using four parasitic elements shows that the null that can be formed is sharper and deeper when the additional elements are added. The array also displays a modest ability to form a lobe (7 dB directivity) towards a desired signal.

The experimental measurements used a general purpose minicomputer with Fortran programming and a slow power measurement device, so that actual elapsed beam-forming times were very slow. An estimate of the convergence time that could be achieved by a microprocessor controller can be made by assuming that the microprocessor cycle time (i.e., a fetch/operation/store cycle) is the limiting factor, rather than the analog-to-digital and digital-to-analog conversion speeds, or the response times of the receiver and reactive loads. Taking an average cycle time of 5 μsec as typical of a fast microprocessor with coprocessor, estimating that each iteration step can be programmed with eight instructions, and taking 40 iterations as typical for convergence, a beam-forming time of 1.6 msec results. Questions relating to stability of the algorithm at these rates are of course yet to be answered.

The main advantage of a RESAA, as compared with a conventional adaptive array, is the elimination of the mixers and other hardware needed to perform the complex weighting of each element's output at an intermediate frequency (IF). In general, a RESAA configuration can be made with substantially fewer components than a comparable conventional adaptive array. It also lends itself (with microstrip elements) to fabrication as an integrated antenna, in which the phase shifter reactive loads are incorporated directly into a multilayered sandwich construction. Another advantage is the necessarily smaller overall size (needed to maintain tight coupling between elements).

There are two disadvantages to the RESAA technique: (1) less control of the pattern is obtainable for the same number of elements, since only one control device is used for each element with the RESAA compared to the two control devices (for full complex weighting) for each element of a conventional adaptive array, and (2) increased control over the pattern cannot be achieved simply by adding more elements, since new elements added at the periphery of the array have progressively less influence on the pattern.

FUTURE WORK

Future research work on the RESAA technique will investigate the following issues and applications.

- Planar array performance. Two-dimensional arrays will be fabricated to determine the ability of a RESAA to beam form in both the azimuth and elevation planes.

- Algorithm development. Other algorithms will be investigated to determine if they produce a faster convergence speed or more robust null. One such possible algorithm is guided random search.[2] This algorithm allows the reactive loads to be adjusted simultaneously, rather than serially; this form of adjustment appears to be essential for larger arrays.

- Bandwidth enhancement. More sophisticated designs for the phase shifter teminations will be investigated to improve their bandwidth and, hence, the nulling bandwidth. If the nulling bandwidth can be substantially improved to approach the array bandwidth, wider band elements will be considered.

- Mutual coupling studies. The mutual impedance between the array elements obviously is essential for the operation of the array and enters the analysis equations in a straightforward manner.[1] However, the mutual impedance matrix entries depend on a variety of factors, such as element spacing, size, shape, and orientation. Hence, the best antenna configuration is not at all obvious. Using the loaded N-port theory,[1,3] the role of the mutual impedance will be examined in detail. One approach is to hold a set of reactive loads fixed and vary the mutual impedance, in effect optimizing array performance in a parameter space made up of the resistive and reactive portions of the mutual impedance. Questions relating to realizability of the optimum point lead to a rather complex problem.

- Hybrid combinations of parasitic elements and driven elements. An interesting possibility is to combine reactively steered parasitic elements — and their control loops — with driven elements controlled in the manner of (1) a conventional phased array or (2) an adaptive array using, for example, a Howells-Applebaum control loop.

---

[3] R. F. Harrington. "Reactively Control Directive Arrays," IEEE Trans. Antennas Propag., Vol. AP-26 (May 1978), pp. 390-397.

Appendix

STEEPEST DESCENT CONTROL ALGORITHM

This appendix gives a detailed description of the steepest descent algorithm, a flow chart of which is shown in Figure A-1.

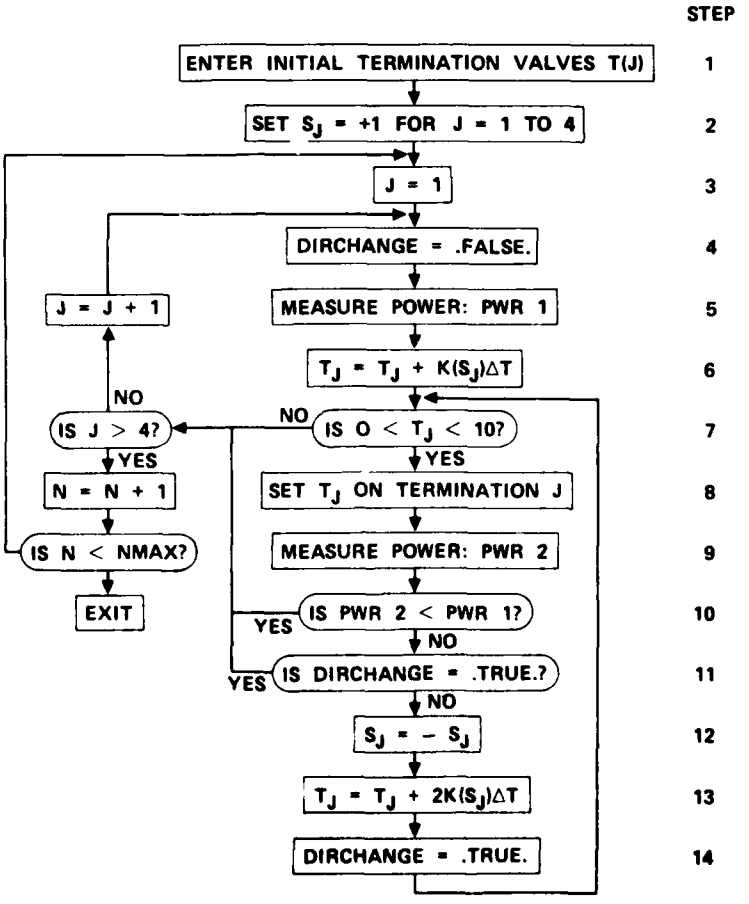

FIGURE A-1. Flow Chart for Steepest Descent Algorithm.

At Step 1 the initial values of the terminations are assumed to be available, either as a result of a random search phase or as a selected set of initial values. The parameter S_J controls the sign of the change in each termination value at each iteration; initially, all of the S_J are set to +1 at Step 2. The iterative loop starts with element 1 (Step 3) by setting a parameter called DIRCHANGE to logical FALSE (Step 4). DIRCHANGE is a toggled parameter that serves to indicate a change in sign in S_J.

At Step 5 the output of the receiver is measured and stored as PWR1. The termination value T_J (in terms of varactor bias voltage applied to the reactive terminations) is then computed in Step 6 according to the steepest descent algorithm given in Equation 1. K is the rate constant, but note that the sign of K is immaterial at this point since S_J can cause the incremental term to be either positive or negative. Steepest ascent or descent is actually determined by the sense of the inequality in Step 10. Before actually setting the computed value of T_J on the termination, the value is checked in Step 7 to ensure that it does not fall outside the control range. In Step 8 the digital-to-analog converter is addressed and the varactor bias voltage is set to the value of T_J.

The new value of received power is then measured and compared with the earlier power reading in Step 10. If the new measured power is lower, the adjustment process passes along to the next element. When the J = 4 element is completed, the adjustment procedure returns to the J = 1 element unless the maximum number of loops given by NMAX is reached, in which case the program ends. For continuous control no check against NMAX is necessary.

If the result of the comparison in Step 10 was such that the new power measurement (PWR2) was greater than PWR1, then S_J must have its sign changed to change the sense of the incremental term in Step 6. First, however, a check is made in Step 11 to see if such a change in sign has already occurred, in which case control is passed to the next element. Step 11 (and the use of the DIRCHANGE variable) is necessary to prevent oscillations at the minimum point or under conditions in which large noise fluctuations can cause the test in Step 10 to fail no matter what sign S_J takes. If the sign change in S_J has not yet occurred (as indicated by the NO result of Step 11), the sign is changed and a new computation of T_J is made in Step 13. The factor of 2 occurs in order to return the value of T_J to its previous value (just prior to entering Step 6) and increment it in the new (opposite) direction. DIRCHANGE is then toggled to TRUE and control passed back to Step 7.

INITIAL DISTRIBUTION

8 Naval Air Systems Command
- AIR-00D4 (2)
- AIR-03C, G. Heiche (1)
- AIR-330B, F. J. Lueking (1)
- AIR-330C, R. Thyberg (1)
- AIR-330D, C. Caposell (1)
- AIR-330E, A. Glista (1)
- AIR-330R, J. Willis (1)

5 Chief of Naval Operations
- OP-0941 (1)
- OP-0944 (1)
- *OP-098 (1)*
- OP-0986 (1)
- OP 987 (1)

7 Chief of Naval Research, Arlington
- ONR-200, J. O. Dimmock (1)
- *ONR-210B, LCDR T. L. Swafford (1)*
- ONR-250, CDR D. S. Siegal (1)
- ONR-414
  - L. Griffiths (1)
  - D. Lewis (1)
  - G. Wright (1)
- ONR-430, A. M. Diness (1)

4 Naval Electronics System Command
- Code 61A (1)
- Code 611, B. Hughes (1)
- Code 614, J. Cauffman (1)
- PME 109-20, R. Eisenberg (1)

4 Naval Sea Systems Command
- SEA-62R1
  - C. E. Jedrey (1)
  - T. Tasaka (1)
- SEA-99612 (2)

1 Commander in Chief, U. S. Pacific Fleet (Code 325)

1 Commander, Third Fleet, Pearl Harbor

1 Commander, Seventh Fleet, San Francisco

3 Naval Air Development Center, Warminster
- A. T. Cerino (1)
- H. H. Heffner (1)
- G. T. Piffung (1)

4 Naval Ocean Systems Center, San Diego
- Code 532, J. H. Richter (1)
- Code 5324, H. A. Wilcox (1)
- Code 534, C. Ramstedt (1)
- Code 8114, P. M. Hansen (1)

2 Naval Postgraduate School, Monterey
- D. Bukofzer (1)
- O. Heinz (1)

7 Naval Research Laboratory
  Code 7500, J. R. Davis (1)
  Code 7550
    D. Himes (1)
    W. Meyers (1)
    L. Wagner (1)
  W. Gabriel (1)
  F. F. Kretschmer (1)
  C. M. Krowne (1)
3 Naval Ship Weapon Systems Enginering Station, Port Hueneme
  Code 5711, Repository (2)
  Code 5712 (1)
1 Naval War College, Newport
1 Office of Naval Research, Pasadena Branch Office (R. Brandt)
1 Office of Naval Technology, Arlington (MAT-073)
1 Pacific Missile Test Center, Pt. Mugu (C. Kaloi)
1 Army Research Office, Research Triangle Park (J. W. Mink)
1 Harry Diamond Laboratories, Adelphi (A. R. Sindoris)
2 Rome Air Development Center, Griffiss Air Force Base
  DCCR, J. A. Graniero (1)
  OCTS, V. Vannicola (1)
1 Rome Air Development Center, Hanscom Air Force Base (R. Mailloux)
12 Defense Technical Information Center
1 California State University, Electrical and Computer Engineering Department, Northridge, CA (E. S. Gillespie)
1 General Atronics Corporation, Philadelphia, PA (L. R. Burgess)
2 Lincoln Laboratory, MIT, Lexington, MA
  J. T. Mayhan (1)
  A. Simmons (1)
1 New Mexico State University, Physical Science Laboratory, Las Cruces, NM (K. R. Carver)
1 Ohio State University, ElectroScience Laboratory, Columbus, OH (R. T. Compton)
1 R. C. Hansen, Inc., Tarzana, CA (R. Hansen)
1 Stanford University, Department of Electrical Engineering, Stanford, CA (B. Widrow)
1 Syracuse University, Department of Electrical and Computer Engineering Syracuse, NY (R. A. Harrington)
2 University of California, Electrical Sciences and Engineering Department Los Angeles, CA
  N. G. Alexopoulos (1)
  R. S. Elliott (1)
1 University of Colorado, Electromagnetics Laboratory, Boulder, CO (D. C. Chang)
1 University of Houston, Department of Electrical Engineerng, Houston, TX (S. A. Long)
1 University of Pennsylvania, Moore School of Electrical Engineering Philadelphia, PA (B. D. Steinberg)
1 University of Texas, Department of Electrical Engineering, Houston, TX (T. Itoh)
1 Zeger-Abrams Inc., Glenside, PA (A. E. Zeger)

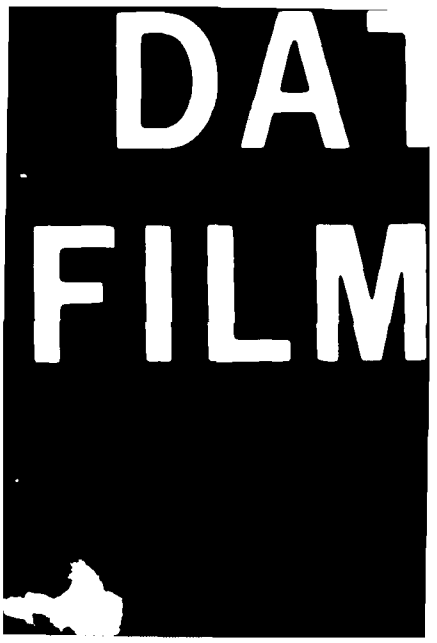
DA
FILM